International Journal of Nanomedicine

Dovepress

open access to scientific and medical research

Open Access Full Text Article

ORIGINAL RESEARCH

A One Step Strategy Based on Hollow Gold Nanoparticles to Detect C-Reactive Protein with High Sensitivity (Hs-CRP) in Serum for Monitoring Cardiovascular Disease

Changyou Luo[1,*], Ruiqing Zhang[2,*], Ji Liu[1,*], Xingyue He[1], Shengzhou Li[1], Chuanjiang Ran[1], Songbo Ma[3], Yan Shen[1]

[1]Department of Pharmaceutics, China Pharmaceutical University, Nanjing, 211100, People's Republic of China; [2]Children's Hospital of Nanjing Medical University, Nanjing, People's Republic of China; [3]Department of Oral and Maxillofacial Surgery, The Affiliated Taizhou People's Hospital of Nanjing Medical University, Taizhou, Jiangsu, 225300, People's Republic of China

*These authors contributed equally to this work

Correspondence: Yan Shen; Songbo Ma, Email shenyan@cpu.edu.cn; masongbo1978@163.com

Purpose: Rapid detection and diagnosis of diseases facilitate timely and effective treatment of cardiovascular diseases (CVD). The establishment of a one-step rapid detection method provides a new method for the initial screening and disease risk assessment of patients with cardiovascular diseases in primary medical units.

Methods: Hollow gold nanoparticles (HGNPs) were synthesized using a cobalt template method followed by use as signal amplification probes for ultra-sensitive quantitative detection of serum C-reactive protein (CRP). To induce the localized surface plasmon resonance (LSPR) and improve protein labeling efficiency, we developed a sensitive detection mode by coating polyvinyl-pyrrolidone (PVP-K30) on the HGNPs, resulting in a significant improvement in detection performance.

Results: Compared to traditional colloidal GNP-based LFTA, PVP-coated HGNPs exhibit a lower visual detection limit of 1 ng/mL, which a 25-fold decrement compare to using GNPs as the antibody-labeled probe, and the detection limit could be reduced to 0.14 ng/mL under the quantitative instrument.

Conclusion: The one-step method based on HGNP immunochromatographic strips modified with PVP established in this study can be used for the detection of CRP and hs-CRP in biological samples. The performance of the immunochromatographic technique designed in this study was evaluated from the perspective of synthetic markers, and the application conditions of this strip were screened, verifying its high specificity, indicating that it has high sensitivity and strong detection limit compared to colloidal gold. The sensitivity of the hollow gold immunochromatographic test strip in this article has been increased by about 25 times, providing a new method for rapid detection of CVD in clinical diagnosis.

Keywords: C-reactive protein, lateral flow immunoassay, hollow gold nanoparticles, in vitro diagnostics, polyvinylpyrrolidone

Introduction

Cardiovascular disease (CVD) is one of the leading causes of death in the world. It is a chronic disease that develops gradually over a lifetime. Symptoms usually occur only in advanced disease, and in severe cases, major cardiovascular events such as acute myocardial infarction, stroke and pulmonary embolism occur. The World Health Organization estimates that CVD causes about 30,000 deaths every day. In China, cardiovascular diseases account for the first place in the total death causes of urban and rural residents, accounting for 46.74% in rural areas and 44.26% in urban areas.[1] With the younger age of tobacco use, poor diet and lack of exercise, cardiovascular diseases are becoming more popular in young ages.[2] The economic burden brought by cardiovascular diseases to residents and society is increasing gradually, and it has become a major public health

Received: 20 September 2023
Accepted: 8 January 2024
Published: 25 January 2024

problem. Therefore, early detection, diagnosis, and treatment are important for slowing the progression of cardiovascular disease to advanced stages and improving overall outcomes. Electrocardiograms and cardiac magnetic resonance (CMR) are often the gold standard for diagnosing certain cardiovascular diseases, but the application of these assistive tools are limited by high cost, high requirements for technical expertise, and is not suitable as a screening tool for the general population.[3,4] This brings a lot of difficulties to early diagnosis of CVD and seriously affects the recovery of patients. In order to break through the current bottleneck, emerging technologies such as immunochromatography and microfluidic technology have the advantages of low cost, simple instruments, and easy integration, and have been developed to a relatively mature level.[4] They play an important role in the early prevention, diagnosis, and treatment of cardiovascular diseases. However, considering the application situation, microfluidic technology still has certain limitations.

Inflammation is an important player in chronic disease and cardiovascular disease.[5] The presence of chronic low-grade inflammation also should be noted because immune senescence during aging leads to a higher incidence of metabolic and cardiovascular complications in the elderly. C-reactive protein (CRP) is an acute reactive protein (APRP) synthesized by the liver that can react with the C-polysaccharide in the Streptococcus pneumoniae capsule.[6] It is part of the non-specific immune mechanism, and its main biological function is to activate the classical pathway of complement by binding to ligands (phosphocholine of apoptotic and necrotic cells, or invading bacteria, fungi, parasites, etc.), enhance leukocytophagocytosis, and stimulate the activation of lymphocytes or monocytes/macrophages as opsonins. Furthermore, serum CRP is an excellent biomarker of CVD and a strong and independent predictor of adverse cardiovascular events.[7,8] These will cause damage to the intima of blood vessels, cause a large release of inflammatory substances, promote the interaction between blood leukocytes and endothelial cells, and thus lead to and promote the occurrence and development of cardiovascular diseases.[9,10] Usually, the concentration of CRP in the serum is very low (<5 mg/L), and CRP rapidly increases when the body experiences infections, tissue damage, and inflammatory diseases. After the disease is cured, the content of CRP rapidly decreases and recovers within a week.[11] In routine clinical tests, CRP is an excellent tool for rapid and early diagnosis of bacterial or fungal infections, with pathological CRP exceeding 10–15 mg/L in the case of infection, the detection range of CRP is generally 10–150mg/L, because the lack of high sensitivity is not enough to predict the normal range of low-degree inflammatory reactions (such as CVD).[12] C-reactive protein with high sensitivity (hs-CRP) is a kind of CRP with higher sensitivity and lower detection limit, which makes the determination of low concentration CRP more accurate.[13]

The most promising biosensing approaches for CVD biomarkers are immunoassays, sandwich immunoassays, and competitive immunoassays, in which either enzyme labels or synthetic agents are used as signal reporters.[14] Lateral flow immunoassay (LFIA) has gained increasing attention and emerged as the most prominent point-of-care test (POCT) in the past two decades with fewer processing steps and shorter analysis time.[15,16] Based on their unique properties, gold nanoparticles (GNPs) have been widely used as a detection probe in LFIA for medical diagnosis, drug testing,[17–19] food safety,[20] and other protein tests. Although the use of GNPs simplifies the detection of biomolecules, traditional GNPs-based LFIA techniques are highly dependent on the visual intensity of GNPs deposited on the membrane surface.[21,22] Moreover, GNPs as probes hardly provide better sensitivity to fit the diagnostic requirement,[23,24] which only could be used to provide qualitative or semi-quantitative results (yes/no or positive/negative) and easily caused a visual error.[25,26] While innovative research efforts continue to improve the detection performance of GNPs-based LFIA, it still cannot be satisfied in the application of key factor detection, such as inflammation or infectious disease diagnosis.

Due to the optical properties of AuNPs being highly dependent on their shape,[27] we proposed HGNPs with a porous and hollow structure could be a potential alternative material for LFIA. Compared to traditional GNPs, HGNPs exhibit greater light extinction performance due to the shell of nuclear resonance between produced electromagnetic field enhancement and local surface plasmon resonance, resulting in the extinction of intense light at visible wavelengths. In addition, the colloid stability of HGNPs is significantly higher than that of GNPs of the same size. The HGNPs with promoted total surface area and increased number of binding sites on the rough surface of hollow gold, which is conducive to improving the conjugation rate of immobilized antibodies. The above advantages allow for a higher signal-to-noise ratio (blue-black/white) and a clearer color signal when the same number of nanoparticles are gathered.

To ensure the colloidal stability of GNPs, the labeled pH is usually more alkaline than the isoelectric point of the protein to be labeled which reduced the binding ability to the target protein due to interrupting the formation of the Au-S bond. Therefore, we consider using polyvinylpyrrolidone (PVP) to improve the colloidal stability of HGNPs. PVP is an amphiphilic

polymer that can be used to disperse nanoparticles in water and organic solvents. PVP coating onto the surface of a colloidal particle as a dispersant shell has been used to stabilize colloidal particles independent of ionic strength, pH value, and solvent polarity,[28] as it can create steric repulsions upon compression of neighboring polymer chains. PVP-coated HGNPs could not only conjugate with antibodies without affecting its activity but also maintain the protein absorption efficiency independent of the protein isoelectric point, suggesting their advantages in LFIA immunochromatography.

In this study, we developed a one-step method based on immunochromatographic strips containing PVP-modified HGNPs (Scheme 1A) as a detection label for the LFIA assay to high sensitivity detection of CRP and hs-CRP in biological samples (Scheme 1B). PVP@HGNPs possess a stronger plasma signal and excellent colloid stability. PVP-coated HGNPs exhibit a lower visual detection limit of 1 ng/mL, which a 25-fold decrement compared to using GNPs as the antibody-labeled probe, and the detection limit could be reduced to 0.14 ng/mL under the quantitative instrument. Our study paves the way for rapid, highly sensitive, and convenient POCT for CRP detection in clinical diagnosis.

Materials and Methods

Materials and Instruments

Chloroauric acid was purchased from Shanghai Chemical Reagent Co., Ltd., sodium borohydride and sodium citrate from Nanjing Chemical Reagent Co., Ltd., bovine serum albumin (BSA), trehalose and phosphate buffered-brine (PBS) from Yuan-Ye Biological Co., Ltd., sodium chloride, sucrose, polyvinylpyrrolidone from Gansu Science Co., Ltd., $CoCl_2$ was purchased from Guangdong Guanghua Sci-Tech Co., Ltd., (Guangdong, China). CRP monoclonal antibody (MC15 and MC18), sheep anti-mouse IgG antibody (GMI06) and CRP standard substances (CRP01) were purchased from Hangzhou Qitai Biotechnology Co., Ltd., Phosphate buffered solution (PBS) was purchased from Jiangsu KeyGEN BioTECH Co., Ltd., All other reagents were analytical grade and were used without further purification.

The sample pad, plastic packing, nitrocellulose (NC) membrane, and absorbent pad were obtained from SARTORIUS Germany. XYZ three-dimensional film spraying instrument and automatic cutting machine were supplied by Shanghai Jinbiao Biological Technology Co., Ltd.

The serum samples were obtained from Department of Cardiology, Affiliated Hospital of Yangzhou University. The blood samples are all leftover from cardiovascular disease patients who have undergone necessary physiological and

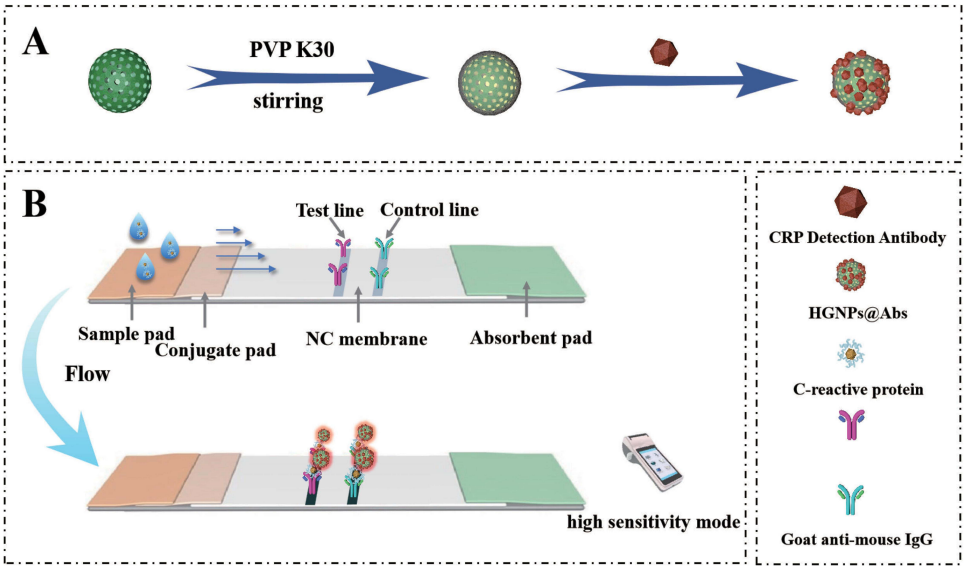

Scheme 1 Schematic demonstration of the process used to detect CRP using HGNPs-LFIA:(**A**) HGNPs@Abs fabrication. After the synthesis of hollow gold nanoparticles, PVPK30 was added for stirring modification, and then CRP detection antibodies were modified for subsequent detection.(**B**) Qualitative analysis platform for the LFIA systems. After the sample is dropped into the sample plate, the CRP in it is different from HGNPs@Abs Binding, as chromatography proceeds, binds to CRP capture antibody on the t-line and develops color for observation of results.

pharmacological analysis in the hospital, and the collection method is consistent with the hospital. All participants gave their written consent prior to being included in the study. The study was conducted according to the guidelines of the Declaration of Helsinki and approved by the Ethics Committee of the School of Pharmacy of China Pharmaceutical University (approval number: 202109001).

Preparation of GNPs and HGNPs

GNPs were prepared using a sodium citrate-reduction method.[29] Briefly, a 1 mL solution of 1% (m/v) sodium citrate was added to 100 mL boiling deionized water. When the mixture was heated to boiling again, a 1 mL solution of 1% (m/v) $HAuCl_4$ was added rapidly by constant stirring. After the color of the solution changed to wine-red (in about 2 min), the solution was boiled for another 10 min. After cooling, deionized water was added until the volume reached 100 mL. The obtained gold colloidal was supplemented with 0.1% (m/v) of P300 and stored at 4 °C.

HGNPs were synthesized by cobalt template method as follows[30,31]: Ultrapure water (100 mL), 2 mL of 0.05 M sodium citrate, and 100 μL of 0.4 M $CoCl_2$ solution were consecutively added to a 250 mL round-bottomed flask. After connecting to a vacuum pump, 1 mL of a 0.13 mM $NaBH_4$ solution was added to the flask, followed by stirring for 10 min until the solution darkened. The reaction system will cool down during this process, and water mist may appear. In this step we first get cobalt nanoparticles. The equation is as follows[32] (1–6):

$$2Co^{2+} + 4BH_4^- + 9H_2O \rightarrow Co_2B + 12.5H_2 + 3B(OH)_3 \quad (1)$$

$$NaBH_4 + 2H_2O \rightarrow NaBO_2(aq) + 4H_2 \quad (2)$$

$$Co^{2+}(aq) + 2NaBO_2 \rightarrow Co(BO_2)_2 + 2Na^+ \quad (3)$$

$$2Co_2B + Co(BO_2)_2 \rightarrow 5Co^0 + 2B_2O_x + O_2 - B_2O_3 \quad (4)$$

$$4Co_2B + 3O_2 \rightarrow 8Co^0 + 2B_2O_3 \quad (5)$$

$$2Co^{2+} + 4BH_4^- + 9H_2O \rightarrow Co_2B + 12.5H_2(gas) + 3B(OH)_3 \quad (6)$$

Metallic *Co* is formed as a Secondary Product. In this process, the preparation of cobalt nanoparticles is the key step. The particle size and concentration of cobalt nanoparticles obtained by reducing cobalt chloride with sodium borohydride under the protection of sodium citrate directly determine the subsequent formation of gold nanoparticles: the particle size of cobalt nanoparticles is too small, and the hollow structure of gold nanoparticles becomes weak and tends to be solid. On the contrary, when the particle size of cobalt nanoparticles is too large, the wall thickness of gold nanoparticles is too thin, the particle size is too large, the shape is irregular, and it is easy to break. We then added 500μL of a 25 mM $HAuCl_4$ solution to the flask for stirring overnight, the solution will gradually turn black purple and exhibit the Tyndall effect. The electrochemical replacement reaction between chloroauric acid and elemental cobalt produces a gold shell which is wrapped on the surface of cobalt nanoparticles, and oxygen is quickly introduced to oxidize the cobalt nanoparticles in the core, thus forming a cavity structure and preparing hollow gold nanoparticles, The equation is as follows (7–9):

$$3Co^0 + 2AuCl_4^- \rightarrow 2Au^0 + 3Co^{2+} + 8Cl^- \quad (7)$$

$$Co^0 + 0.5O_2 \rightarrow CoO \quad (8)$$

$$3CoO + 0.5O_2 \rightarrow Co_3O_4 \quad (9)$$

Followed by the addition of 100 μL of a 20% (w/w) polyvinylpyrrolidone (PVP K30) solution to the reaction and stirring for 30 min. The final reaction solution was centrifuged for 15 min at 10000 r/min at 4 °C, the supernatant was discarded, and the precipitate was re-suspended with ultrapure water and stored at 4 °C until use.

Characterization of HGNPs and GNPs

The HGNPs and GNPs particle size distribution was determined by dynamic light scattering on a Zetasizer Nano-ZS90 analyzer (Malvern Instruments, Malvern, UK). The zeta potentials of prepared HGNP solutions also were determined by a Zetasizer Nano-ZS90 analyzer. The absorption spectra of HGNPs and GNPs, ranging from 400 nm to 900 nm, were obtained using a UV-vis spectrophotometer (cat # 8453; Agilent Technologies, Santa Clara, CA, USA) at 25 °C. The morphology observation of the synthesized HGNPs and GNPs was characterized by transmission electron microscopy (TEM) (HT7700; Hitachi, Tokyo, Japan) using a charge-coupled device camera operating at an accelerating voltage of 100 kV.

Preparation of GNPs and HGNPs Labeled CRP detection antibody

The labeling procedure for the MC18 protein coupled to GNPs follows these steps. First, 1 mL of the GNPs solution was adjusted to pH 8.5 using 0.1 M K_2CO_3 solution, after which 25 μL of 0.2 mg/mL MC18 protein solution in PBS was added to the GNPs solution and incubated for 25 mins. After adding 10% BSA 100μL and incubating for 20 mins, the GNPs suspension was centrifuged at 7500 rpm for 20 mins at 4 °C. The precipitate of the GNP-labeled MC18 protein was resuspended in 50 μL of stabilizing buffer (20 mM Tris (pH 9.2), 0.3% sucrose, and 0.05% PEG 20000) and stored at 4 °C until use. Reaction efficiency of the antibody was calculated using Equations (10).

$$RE(\%) = \frac{A_0 - A_s}{A_0} \times 100\% \tag{10}$$

Where A_0 is the total mass of the added antibody, and As is the mass of the antibody in the supernatant.

Labeling of the CRP monoclonal antibody MC18 protein with HGNPs was performed as described previously, with minor modifications. Briefly, 1 mL of the HGNPs solution was adjusted to pH 3.0 using 0.1 M HCl solution, 10 μL of a 0.2 mg/mL MC18 solution in PBS was added to a 1 mL 0.05 mg/mL HGNPs solution and incubated for 20 mins. We then added 10% BSA 100 μL and incubate for 20 mins, followed by centrifugation at 8500 rpm for 15 min at 4 °C. The HGNPs precipitate was resuspended in 50 μL of the stabilizing buffer (3%BSA, 5% trehalose, 5% sucrose, 0.1% P300 in 0.01 M Tris-HCl) and stored at 4 °C until use.

Determination of the Time for Hollow Gold Labeled Antibodies

Adequate reaction time can ensure that the antibody is firmly coupled to the hollow gold surface, but prolonged incubation time can lead to increased non-specific adsorption. Therefore, we need to choose an appropriate reaction time. In this study, we investigated the T line, C line, and OD_T/OD_C changes at 10, 15, 20, 25, and 30 minutes of labeling time to determine the optimal labeling time.

Determination of Sealing Time for Hollow Gold Nanoparticles

Sealants can reduce non-specific binding and the occurrence of false positives, but prolonged closure can also affect experimental results. In this study, we investigated the changes in T line, C line, and OD_T/OD_C at 10, 15, 20, 25, and 30 minutes of labeling time to determine the optimal labeling time.

Preparation for LFIA

LFIA preparation was carried out as previously described.[33,34] The LFIA has the following sections: NC membrane, plastic packing, conjugate pad, sample pad, and absorbent pad. The conjugate pad was treated with a buffer (3% BSA, 5% trehalose, 5% sucrose, and 0.1% P300 in 0.01 M Tris-HCl; pH=6.5) and dried at 60 °C for 2 h. Similarly, the sample pad was treated with a buffer (0.2% BSA, 1% trehalose, 5% sucrose, 0.3% PVP K30, and 0.1% P300 in 0.01M Tris-HCl) and dried at 60 °C for 2 h. The detector reagent (HGNPs@MAb conjugate) was applied onto the conjugate pad using a BioDot platform at a jetting rate of 7.5 μL/cm and dried at 37 °C for 30 min. The capture reagent (CRP MAb conjugate) and goat anti-mouse IgG antibody were composed of T and C lines positioned at a 7-mm interval. The CRP MAb conjugate (1.5 mg/mL) and goat anti-mouse antibody (1.7 mg/mL) were spotted into the NC membrane at 0.9 μL/cm and 0.8 μL/cm, respectively, to form the T and C lines. The NC membrane was dried at 37 °C under a vacuum for 3

h. Using a ZQ2002 guillotine, the NC membrane, the probe-conjugated pad, the sample pad, and the absorbent pad were subsequently attached to the plastic backing and cut into 4 mm wide immunochromatographic strips. The obtained LFIA was then stored at 25 °C in silica gel (desiccant)-containing plastic bags.

Preparation of CRP and Samples

For HGNPs-LFIA, a series of concentration gradients were designed. A standard CRP solution was prepared by adding standard CRP to 0.01 M PBS at final concentrations of 0 (as a negative control), 0.25, 0.5, 1.0, 2.5, 5.0, 7.5, 10.0, 25.0, 50.0, 75.0, and 100.0 ng/mL. For GNPs-LFIA, the concentration gradient ranges from 0 (as a negative control), 5.0, 7.5, 10.0, 25.0, 50.0, 75.0, 100.0, 125.0, 150.0, 200.0, and 250.0 ng/mL.

Collection of CRP Serum Samples

CRP levels in human serum samples were detected using the same protocol. To produce samples with values within the dynamic range of the measurement, plasma or serum samples must be diluted 1:1000 with 0.01 M PBS sample dilution buffer. Plasma samples were obtained by centrifuging at 2500 *g* for 15 min at 4 °C, and serum samples were stored at −80 °C.

CRP Quantification Using the HGNPs-LFIA

To demonstrate the sensitivity of the HGNPs-LFIA platform, CRP protein was quantified using the HGNPs-LFIA system. Briefly, 120 μL of CRP standard solution at varying concentrations (in 0.01 M PBS) were added to the well of the sample pad. Following 15 min of incubation, the optical density (OD) values of the test (OD_T) and control (OD_C) lines were determined using an optical quantitative analyzer (Wuhan Zhongrui Biotechnology Co., Ltd., China). The CRP quantitative analysis standard curve was established by plotting the (OD_T/OD_C) curve.

To obtain analytical sensitivity, we assessed limit-of-detection (LOD), which is defined by the American Chemical Society as the lowest reliably detectable concentration. There are common LOD calculation methods when a calibration curve is already available. IUPAC Method.[35] by Eq. (11):

$$X_L = \bar{X}_B + Ks_B,\ C_L = ks_B/m \tag{11}$$

Here, X_L is the smallest measure (signal at LOD), $\bar{X}_B$ is the mean blank signal, and k is a numerical factor chosen following the confidence level (K = 3 for 99.86%, K = 2 for 97.7% with normal distribution), S_B is the mean blank sample standard deviation, m is the slope of the calibration curve, and C_L is the LOD.

Statistical analysis was performed using Bland-Altman methods[36,37] (comparing two groups of data detected by immunoturbidimetry and HGNPs-LFIA) with a minimum confidence level of 0.05 for significant statistical differences. All values are reported in terms of mean and standard deviation.

Statistic Analysis

Statistical analysis was performed using a standard Student's *t*-test and One-Way ANOVA with a minimum confidence level of 0.05 for significant statistical differences. All values are reported in terms of mean and standard deviation. Data were expressed as mean ± SD and at least triplicate independent experiments were carried out. Data were analysed using Prism 8.0 software (GraphPad, La Jolla, CA).

Results and Discussion

The optical and colloidal properties of GNPs are critical for the sensitivity and stability of the LFIA assay. However, the size and shape of GNPs have a significant impact on the surface plasma resonance (SPR) band, colloidal stability, color, and optical absorption intensity. In this study, conventional GNPs and HGNPs were synthesized using citrate reduction and cobalt template methods, respectively.[29–31]

GNPs and HGNPs had maximum SPR absorptions at 528 and 607 nm, respectively, which is consistent with the optical color observed (red and blue for GNPs and HGNPs, respectively) (Figure 1A). The extinction coefficient of HGNPs increases approximately 2.62-fold at the same concentration, the concentration of HGNPs is determined by Atomic Absorption Spectroscopy (AAS) and was 47.71±0.30 μg/mL. To further assess colloidal stability, all GNP

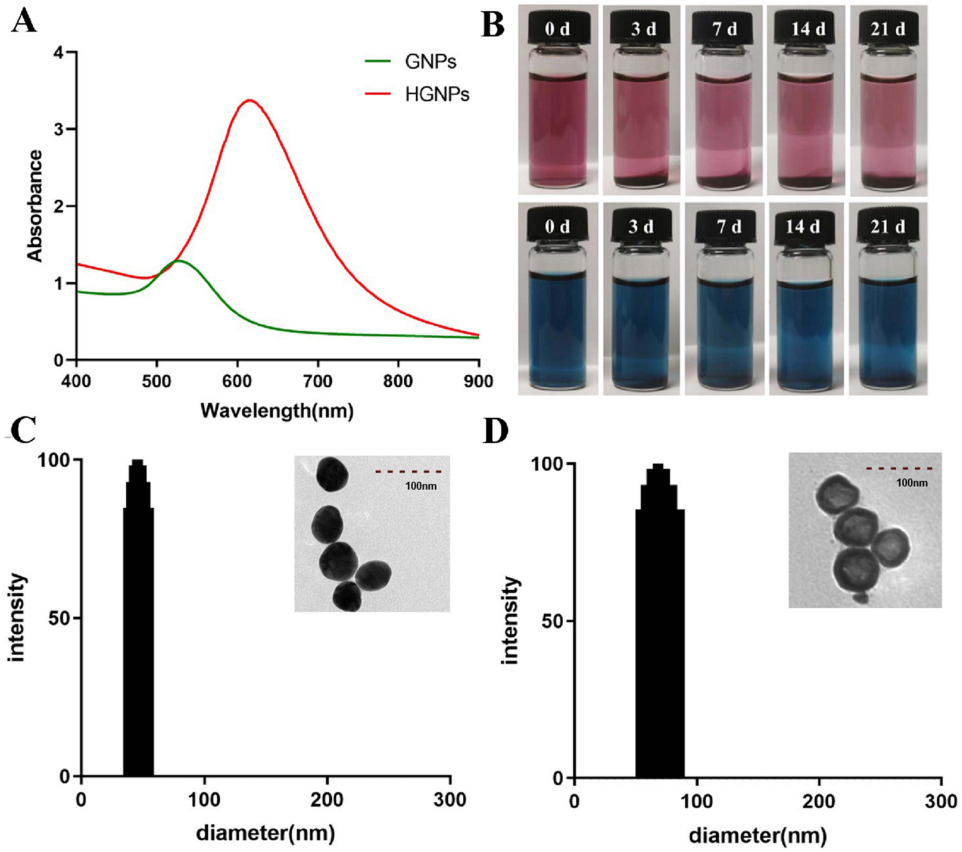

Figure 1 (**A**) At the same concentration (0.05mg/mL), the absorption spectrum of the GNPs and HGNPs. (**B**) Colloidal stability of HGNPs and GNPs (0, 3, 7, 14 and 21 days). (**C**) Size distribution and TEM image (insert) of the GNPs. (**D**) Size distribution and TEM image (insert) of the HGNPs.

solutions were long-term stored at room temperature. As shown in Figure 1B, GNPs had clear stratification after 21 days of storage, whereas the HGNPs exhibited no flocculation or aggregation in the solution. It indicates that GNPs have slight sedimentation aggregation, while HGNPs have a certain stabilizing effect due to the modification of PVP, and the aggregation phenomenon is not obvious. Figure 1C and D show the size distribution of GNPs and HGNPs as determined by the Zetasizer Nano-ZS90 analyzer using dynamic light scattering. The average particle sizes of GNPs and HGNPs were determined to be 21.40 ± 0.854 nm and 69.263 ± 1.737 nm, respectively, with polydispersity indices of 0.342 ± 0.023 and 0.164 ± 0.015. TEM images revealed that the resultant GNPs were relatively uniform spheres, whereas the synthesized HGNPs were uniform and orderly hollow nanospheres with a rough surface and a 5 mm thick PVP layer.

It was found that the pH of the reaction buffer and the surface chemistry properties of the GNPs could influence the adsorption and bioactivity of antibodies.[38] The characteristics and immunoreaction dynamics of HGNPs@Abs were shown in Figure 2. The labeling efficiency of the protein was qualitatively investigated by Sodium dodecyl sulfate-polyacrylamide gel electrophoresis (SDS-PAGE) under different pH conditions, SDS-PAGE results are shown in Figure 2A. pH=5.5 is a labeled environment that has not been acidified, two bands appeared at 55 and 30 kDa, which represent the heavy chain, C_H1, and the light chain, V_H, of anti-CRP Abs respectively, which was reduced by 2-mercaptoethanol in the loading buffer. Anti-CRP Abs standard also yielded two bands, which were not detected in samples containing unlabelled HGNPs, indicating that the surfaces of the HGNPs were successfully modified with anti-CRP Abs. In addition, it has the deepest band color under acidification pH=3.0, which indicates that the labeling efficiency is the highest under this condition. The effect of the pH of the HGNPs on the sensitivity of the strip during labeling is shown in Figure 2B. The optical density of the C line and T line was significantly enhanced after acidification with HCl, with a maximum pH of 3.0. However, significant differences in OD_T/OD_C values were not found when the pH varied between 2.0 and 4.5. This is consistent with the results indicated by SDS-PAGE. The aforementioned findings support the utilization of a running buffer with a pH value of 3.0 for the recognition of

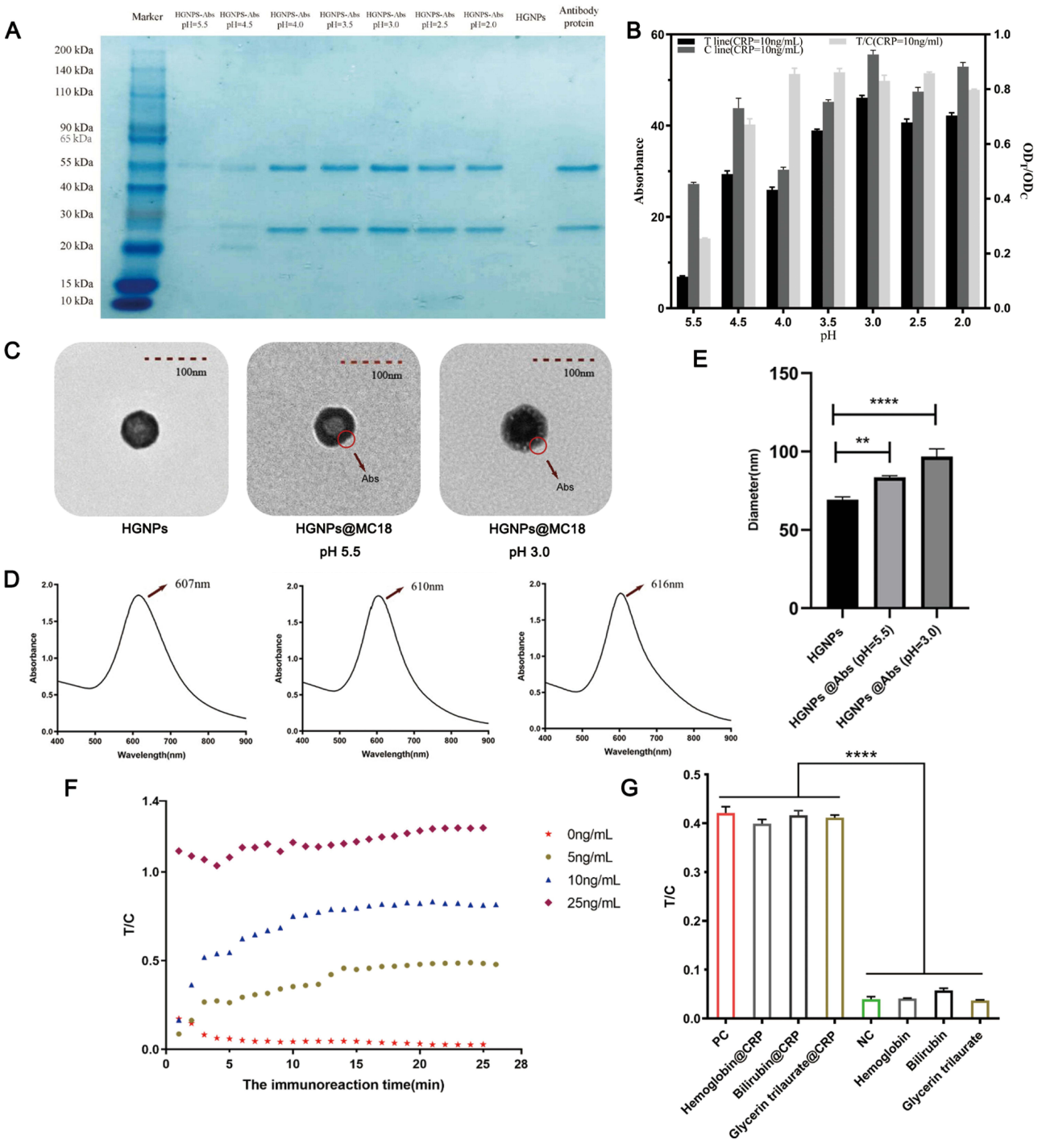

Figure 2 (**A**) SDS-PAGE analysis of HGNPs@Abs under different label pH conditions. (**B**) Effects of label pH value on the ratio of OD_T/OD_C. (n=3) (**C**) TEM image of the HGNPs@Abs. (**D**) the surface plasmon bands of HGNPs and HGNPs@Abs probes. (**E**) Size distribution of the HGNPs and HGNPs@Abs. (n=3, ***P*<0.01, *****P*<0.0001) (**F**)Immunoreaction dynamics of OD_T/OD_C at different CRP spiked concentrations (0, 5.0, 10.0 and 25.0 ng/mL). (**G**) The selectivity of the HGNPs-LFIA assay for three potential cross-reactant samples. (n=3, *****P*<0.0001).

HGNPs@Abs probes and CRP protein. These data indicate that, under the action of PVP, HGNPs remain stable in a strong acid environment, and because the pH of the solution is below the isoelectric point of the protein, the antibody to be labeled can be combined with HGNPs via strong electrostatic adsorption, which significantly improves the labeling efficiency of HGNPs.

The orientation of immobilized antibodies influences the possibility and efficiency of their interaction with antigenic sites.[39] In the corresponding TEM, it could be seen that under optimal labeling conditions, the antibody adhered to the surface of the HGNPs, forming a uniform distribution like flowers (Figure 2C). The surface plasmon bands of HGNPs@Abs were broadened and the red-shift was 9 nm (607–616nm) under optimal labeling conditions, the corresponding redshift was only 6nm (607–610nm) in the unacidified condition (Figure 2D). This was due to modification by the antibody, which changes the refractive index around the HGNPs.[40] Figure 2E showed the size distribution of HGNPs and HGNPs@Abs under unacidified and optimal pH conditions as determined by the Zetasizer Nano-ZS90 analyzer using dynamic light scattering. The average particle sizes of HGNPs, HGNPs@Abs (pH=5.5), and HGNPs@Abs (pH=3.0) were determined to be 69.263 ± 1.737 nm, 83.507 ± 0.995 nm, and 96.810 ± 4.932 nm. The above evidence was sufficient to confirm the previous findings and indicates that the anti-CRP Abs were successfully attached to the surface of the HGNPs. The connection ratio between CRP antibody protein and Au under the mark condition of pH=3.0 was 72.3 ± 9.0%, but in the pH=5.5 labeled environment, the protein binding rate was only 32.0 ± 4.6%. So we select the condition of pH=3.0 as the label environment in subsequent operations. At the same time, by adding the amount of antibodies and the binding rate between antibodies and gold nanoparticles, it can be calculated that the amount of antibody labeling under the optimal pH conditions is 3.615 ± 0.450 ug.

The main factors affecting the sensitivity of immunochromatographic strips are (1) the number of mAbs on the surface of the HGNPs; (2) the volume of the mAbs-HGNPs in the conjugate pad; and (3) the concentration of the captured antibody conjugate on the test line. Therefore, an orthogonal $L9^3$ test was performed to optimize the aforementioned parameters.[41] The ODs on the test and control lines, as well as the OD_T/OD_C ratio, were used to determine the optimal parameters. The orthogonal test analysis results presented in Table 1 demonstrate that the optimal combination was as follows:

The interpretation time may influence the accuracy of the quantitative analysis. To determine the optimal time for interpretation, kinetic curves of the OD_T/OD_C against immunoreaction time were established under varying CRP spiked concentrations. As shown in Figure 2F, the ratio of OD_T/OD_C reached a constant value after 15 min of run time, despite higher CRP concentrations. These results indicate that the 15-min incubation was necessary for LFIA quantitative analysis.

From the experimental results in Table 2, it can been seen that the labeling time of antibodies is not necessarily better, but rather there exists an optimal labeling time. This might be because when the time is too long, some non-target binding takes advantage, thereby weakening the binding of the target protein to our hollow gold sensor. After considering the brightness of the C-line and T-line as well as the OD_T/OD_C value, we chose an antibody labeling time of 25 minutes.

From the experimental results in Table 3, it can been seen that the incubation time of the sealing agent is not necessarily better, but rather there exists an optimal time. It can be found that after 20 minutes, the OD_T/OD_C value does not significantly increase, but the stability also decreases. After considering the SD value and OD_T/OD_C value, the sealing agent incubation time is selected as 20 minutes.

Table 1 The Analysis Results of the Orthogonal Test (HGNPs)

No	The Volume of MC18-HGNPs (μL)	The Quality of Detection Antibody (μg)	The Concentration of Capture Antibody (μL/cm)	The ODs of Test Lines	The ODs of Control Lines	OD_T/OD_C (%)
1	1.5	1.5	1.3	30.3	114.2	0.2653
2	1.5	2	1.5	32.2	111.3	0.2893
3	1.5	2.5	1.7	34.0	109.9	0.3093
4	3.0	1.5	1.7	44.7	118.2	0.3781
5	**3.0**	**2**	**1.5**	**50.3**	**122.8**	**0.4096**
6	3.0	2.5	1.3	43.9	123.4	0.3557
7	4.5	1.5	1.5	48.1	124.9	0.3851
8	4.5	2	1.7	49.5	123.5	0.4008
9	4.5	2.5	1.3	47.3	126.5	0.3739

Note: The bold font represents the optimal parameters of the HGNPs-LFIA.

Table 2 Results of Screening for Antibody Incubation Time

No.	Mark Time(mins)	The ODs of Test Lines	The ODs of Control Lines	OD_T /OD_C(%)	SD
1	10	35.8	64.5	0.5550	0.0051
2	15	45.75	74.73	0.6041	0.0048
3	20	46.33	76.56	0.6051	0.0039
4	**25**	**49.43**	**78.3**	**0.6312**	**0.0125**
5	30	48.10	80.75	0.5956	0.0090

Note: The bold font represents the optimal parameters of the HGNPs-LFIA.(n=3).

Table 3 Screening Results of Incubation Time for Sealing Agents

No.	Incubation Time(mins)	The ODs of Test Lines	The ODs of Control Lines	OD_T /OD_C(%)	SD
1	10	11.20	49.50	0.2263	0.0022
2	15	14.20	54.90	0.2586	0.0063
3	**20**	**19.33**	**60.58**	**0.3191**	**0.0008**
4	25	17.83	55.47	0.3214	0.0068
5	30	18.62	57.76	0.3223	0.0053

Note: The bold font represents the optimal parameters of the HGNPs-LFIA.(n=3).

To further evaluate the potential cross-reactivity of the HGNPs-LFIA platform in CRP protein detection, three samples of potential cross-reactants (hemoglobin, bilirubin, and glycerin trilaurate) were tested. No false-positive results were observed, indicating that the developed HGNPs-LFIA platform for CRP detection is highly specific (Figure 2G).

As a marker of cardiovascular disease (CAD), CRP indicates the risk of CAD when its serum concentration ranges from 1 μg/ mL - 10 μg/mL,[42] the critical value is 1μg/mL. In order to reduce non-specificity during the actual test, the sample is diluted one thousand times with PBS, so the corresponding critical value is 1ng/mL. This requires that the sensitivity of the detection technology can reach 1ng/mL, which is to achieve a balance between specificity and practical detection needs. Figure 3A presented images of HGNPs-LFIA and GNPs-LFIA strips for various concentrations of CRP in PBS under optimal experimental conditions. The HGNPs-LFIA stereogram demonstrates that the blue band on the test line becomes stronger as the CRP concentration increases from 0 ng/mL to 100 ng/mL. In the case of GNPs-LFIA, it was 0 ng/mL to 250 ng/mL, indicating that the visual dynamic detection limit of HGNPs-LFIA was 1 ng/mL, while GNPs-LFIA was 25 ng/mL. From the visual inspection line results, it can be seen that hollow gold has a very excellent improvement in sensitivity compared to colloidal gold, which means that hollow gold can be applied to more flexible scenarios and has a great market prospect. The proposed HGNPs-LFIA displays linearity over the range of 1 – 100 ng/mL in high sensitivity mode, and the calibration equation was determined to be $y=130.11x^2-48.164x+3.9458$ with a reliable correlation coefficient ($R^2=0.9831$). The error bars are based on three duplicate measurements at different CRP concentrations. We found that the HGNPs-LFIA platform has a simple and accurate linear relationship at low concentrations. The calibration equation was determined to be $y=22.289x-0.144$ with a reliable correlation coefficient ($R^2=0.9971$) in the range of 0–10 ng/mL (Figure 3B–D). In comparison, the calibration curve of GNPs-LFIA was also plotted under optimal experimental conditions. The calibration equation was determined to be $y=0.0026x+0.0779$ with a reliable correlation coefficient ($R^2=0.9792$) in the range of 0 – 250 ng/mL (Figure 3E and F). These results demonstrated that using HGNPs as a colored probe instead of conventional 20 nm GNPs increased the sensitivity of the LFIA for CRP detection by approximately 25-fold.

The precision and accuracy of the developed HGNPs-LFIA were evaluated by analyzing the recoveries of three spiked extracts with CRP final concentrations of 1 ng/mL, 5 ng/mL, and 10 ng/mL. Experimental results shown in Table 4 indicate that the average recoveries (n=5) for intra-assay trials ranged from 94.8% to 111.0% with CVs ranging from 3.5% to 14.3%, while the inter-assay recoveries ranged from 87.6% to 95.0% with CVs from 9.1% to 12.6%. The acceptable recoveries and low CV reveal that the new HGNPs-LFIA system is suitable for CRP quantitative analysis.

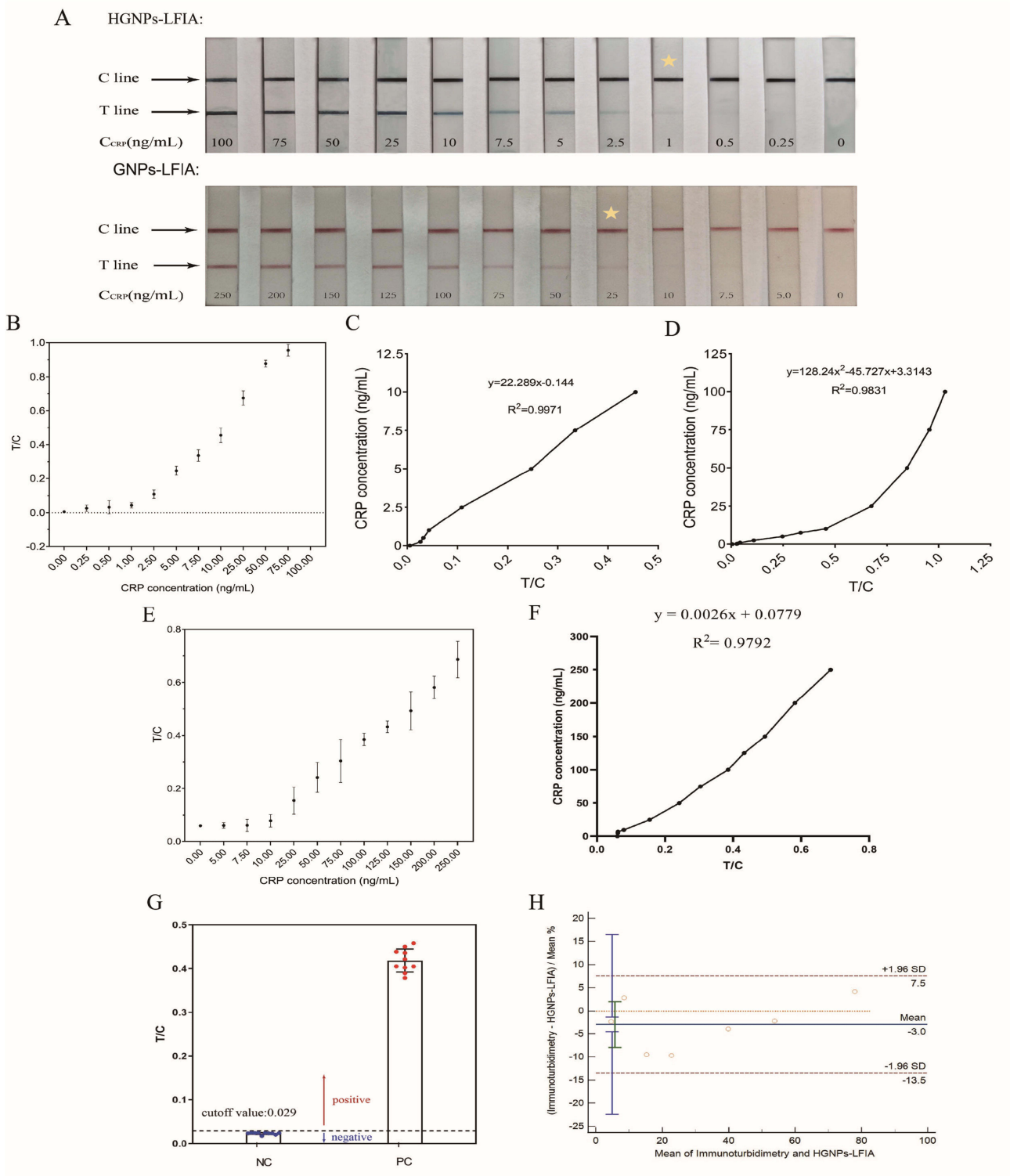

Figure 3 (**A**) Representative photographs are taken from the LFIA of CRP standards. The asterisks indicate detection limits by the naked eye. (**B**) Calibration curves of the HGNPs-LFIA strips for different concentrations of CRP. Fit curve of HGNPs-LFIA, 1–10ng(**C**), 1–100ng(**D**). (**E**) Calibration curves of the GNPs-LFIA. (**F**)Fit curve of GNPs-LFIA. (**G**) Determination of the cutoff value of HGNPs-LFIA for serum CRP detection through mean test value of NC+3 standard deviation (SD). (**H**) A Bland-Altman methods analysis between HGNPs-LFIA and immunoturbidimetry methods in the detection of serum CRP for Seven clinical samples at different concentrations (95% confidence intervals).

To validate the sensitivity of HGNPs-LFIA detection in plasma, normal human serum was used as a negative control (NC), and a serum sample with an appropriate amount of CRP standard (10 ng/mL) as a positive control (PC) in the HGNPs-LFIA assay. The LOD for serum CRP was 0.14 ng/mL based on the mean concentration plus 3 times the

Table 4 The Precision and Accuracy of the HGNPs-LFIA

Sample (ng/mL)	Intra-Assay Precision			Inter-Assay Precision		
	Mean ± SD (ng/mL)	Accuracy (%)	CV (%)	Mean ± SD (ng/mL)	Accuracy (%)	CV (%)
1	1.11 ± 0.09	111.0%	8.1%	0.95 ± 0.12	95.0%	12.6%
2.5	2.37 ± 0.23	94.8%	9.7%	2.19 ± 0.24	87.6%	10.9%
10	10.28 ± 0.36	102.8%	3.5%	9.30 ± 0.85	93.0%	9.1%

Table 5 Accuracy of HGNPs-LFIA in Detecting Clinical Serum Samples

Sample No.	Immunoturbidimetry (ng/mL)	HGNPs-LFIA (ng/mL)	Relative Deviation
1	4.59	4.70±0.74	2.51%
2	8.67	8.43±1.44	−2.75%
3	14.62	16.07±2.98	9.92%
4	21.72	23.93±3.46	10.44%
5	39.02	40.60±7.23	4.10%
6	53.14	54.36±6.87	2.57%
7	79.53	76.31±5.06	−3.41%

Notes: Serum samples were obtained from the Affiliated Hospital of Yangzhou University. The measurement result is the concentration of CRP. When measuring HGNPs LFIA, all samples measure three times in parallel.

standard deviation from 10 negative CRP samples (Figure 3G), which is approximately 170 times better than the visual LOD (vLOD; 25 ng/mL) previously reported for GNPs-LFIA.

To validate the diagnostic accuracy of the HGNPs-LFIA technique, seven clinical plasma samples were collected from the Affiliated Hospital of Yangzhou University. The immunoturbidimetry diagnostic kit was used as a reference. Immunoturbidimetry was used to determine the various concentrations of CRP in plasma. Human serum with varying concentrations of CRP was applied to HGNPs-LFIA under optimized conditions. The samples containing human CRP spiked in serum that had been diluted by a factor of 1000 in PBS were used to perform the CRP detection experiments. The results presented in Table 5 indicate that the two methods had a positive correlation (r=0.987). A Bland-Altman methods analysis as shown in Figure 3H, the consistency limit of the Bland Altman method (−7.9332, 1.9906) did not exceed the professional value of −13.5 to 7.5, indicating that the CRP level in serum in the 7 clinical serum samples showed a very strong concordance between the HGNPs-LFIA and Immunoturbidimetry test results. These findings suggest that the proposed method has a high potential for analyzing CRP levels directly in clinical plasma samples.

To the best of our knowledge, HGNPs were introduced as a signal-amplification reagent for LFIA systems due to their large size, high molar extinction coefficient, and outstanding colloidal stability. Under optimized conditions, HGNPs-LFIA were found to be 25 times more sensitive than GNPs as a colored probe. The LOD of the proposed quantitative strip was found to be as low as 0.14 ng/mL for CRP. Therefore, the HGNPs can be used as a novel signal-amplification probe in LFIA systems, with great potential for use in the ultra-sensitive detection of chemicals in clinical diagnostics.

Conclusion

The LFIA platform has been widely used in various aspects such as cardiovascular disease and other diseases, including disease prevention, diagnosis, treatment, and prognosis. However, there are still some problems, such as false positives caused by non-specific binding, difficulty in meeting detection requirements due to the optical properties of colloidal gold itself, and issues with specificity and stability. These can affect the accurate judgment of disease progression, ultimately leading to delayed diagnosis of the disease and poor prognosis. Compared to commonly used colloidal gold, hollow gold has a larger particle size, is less prone to aggregation, and is a porous structure with a larger specific surface area and

greater affinity for functional molecules. Therefore, it can significantly increase the loading capacity of functional molecules, thereby improving the detection threshold of disease markers and avoiding the occurrence of false positives. We utilized the characteristics of hollow gold to develop an HGNPs LFIA platform based on hollow gold nanomaterials, and studied the process parameters. The HGNPs-LFIA platform we developed will be applied to the detection of serum CRP protein in patients with cardiovascular diseases. The results showed that the detection sensitivity of the HGNPs LFIA platform was 25 times higher than that of colloidal gold (GNPs LFIA platform), and it had a good linear relationship and specificity, which indicates that our developed HGNPs LFIA platform is an excellent serum CRP detection strategy. In addition, due to the simple synthesis and low manufacturing cost of hollow gold nanoparticle materials, as well as the convenient detection methods of the developed HGNPs LFIA platform, this means that hollow gold test strips (HGNPs LFIA platform) have huge market prospects and competitive advantages.

Acknowledgments

We thank Bullet Edits Limited for the linguistic editing and proofreading of the manuscript.

Disclosure

The authors report no conflicts of interest in this work.

References

1. Report TW, Health OC, China DIReport on cardiovascular health and diseases in China 2021: an updated summary. *Biomed Environ Sci*. 2022;35(7):573–603. doi:10.3967/bes2022.079
2. Andersson C, Vasan RS. Epidemiology of cardiovascular disease in young individuals. *Nat Rev Cardiol*. 2018;15(4):230–240. doi:10.1038/nrcardio.2017.154
3. Qin C, Murali S, Lee E, et al. Sustainable low-field cardiovascular magnetic resonance in changing healthcare systems. *Eur Heart J Cardiovasc Imaging*. 2022;23(6):e246–e260. doi:10.1093/ehjci/jeab286
4. Ma Y, Liu C, Cao S, Chen T, Chen G. Microfluidics for diagnosis and treatment of cardiovascular disease. *J Mater Chem B*. 2023;11(3):546–559. doi:10.1039/d2tb02287g
5. Liberale L, Badimon L, Montecucco F, Lüscher TF, Libby P, Camici GG. Inflammation, aging, and cardiovascular disease: JACC review topic of the week. *J Am Coll Cardiol*. 2022;79(8):837–847. doi:10.1016/j.jacc.2021.12.017
6. Kohli R, Bansal E, Gupta AK, Matreja PS, Kaur K. To study the levels of C - reactive protein and total leucocyte count in patients operated of open and laparoscopic cholecystectomy. *J Clin Diagn Res*. 2014;8(6):Nc06–8. doi:10.7860/jcdr/2014/7094.4487
7. Williams ES, Shah SJ, Ali S, Na BY, Schiller NB, Whooley MA. C-reactive protein, diastolic dysfunction, and risk of heart failure in patients with coronary disease: heart and soul study. *Eur J Heart Fail*. 2008;10(1):63–69. doi:10.1016/j.ejheart.2007.11.003
8. Carrera-Bastos P, Fontes-Villalba M, Gurven M, et al. C-reactive protein in traditional melanesians on Kitava. *BMC Cardiovasc Disord*. 2020;20(1):524. doi:10.1186/s12872-020-01812-7
9. Kadoglou NP, Gkontopoulos A, Kapelouzou A, et al. Serum levels of vaspin and visfatin in patients with coronary artery disease-Kozani study. *Clin Chim Acta*. 2011;412(1–2):48–52. doi:10.1016/j.cca.2010.09.012
10. Schumski A, Ortega-Gómez A, Wichapong K, et al. Endotoxinemia accelerates atherosclerosis through electrostatic charge-mediated monocyte adhesion. *Circulation*. 2021;143(3):254–266. doi:10.1161/circulationaha.120.046677
11. Braig D, Nero TL, Koch HG, et al. Transitional changes in the CRP structure lead to the exposure of proinflammatory binding sites. *Nat Commun*. 2017;8(1):14188. doi:10.1038/ncomms14188
12. Moutachakkir M, Lamrani Hanchi A, Baraou A, Boukhira A, Chellak S. [Immunoanalytical characteristics of C-reactive protein and high sensitivity C-reactive protein]. Caractéristiques immunoanalytiques de la protéine C-réactive et de la protéine C-réactive ultrasensible. *Ann Biol Clin*. 2017;75(2):225–229. French. doi:10.1684/abc.2017.1232
13. Nanri A, Moore MA, Kono S. Impact of C-reactive protein on disease risk and its relation to dietary factors. *Asian Pac J Cancer Prev*. 2007;8(2):167–177.
14. Mani V, Durmus C, Khushaim W, et al. Multiplexed sensing techniques for cardiovascular disease biomarkers - A review. *Biosens Bioelectron*. 2022;216:114680. doi:10.1016/j.bios.2022.114680
15. Liu D, Wang J, Wu L, et al. Trends in miniaturized biosensors for point-of-care testing. *TrAC Trends Anal Chem*. 2020;122:115701. doi:10.1016/j.trac.2019.115701
16. Shrivastava S, Trung TQ, Lee NE. Recent progress, challenges, and prospects of fully integrated mobile and wearable point-of-care testing systems for self-testing. *Chem Soc Rev*. 2020;49(6):1812–1866. doi:10.1039/c9cs00319c
17. Fu X, Xie R, Wang J, et al. Development of colloidal gold-based lateral flow immunoassay for rapid qualitative and semiquantitative analysis of ustiloxins a and b in rice samples. *Toxins*. 2017;9(3):79. doi:10.3390/toxins9030079
18. Wu S, Liu L, Duan N, Li Q, Zhou Y, Wang Z. Aptamer-based lateral flow test strip for rapid detection of zearalenone in corn samples. *J Agric Food Chem*. 2018;66(8):1949–1954. doi:10.1021/acs.jafc.7b05326
19. Frohnmeyer E, Tuschel N, Sitz T, et al. Aptamer lateral flow assays for rapid and sensitive detection of cholera toxin. *Analyst*. 2019;144(5):1840–1849. doi:10.1039/c8an01616j
20. Singh J, Sharma S, Nara S. Evaluation of gold nanoparticle based lateral flow assays for diagnosis of enterobacteriaceae members in food and water. *Food Chem*. 2015;170:470–483. doi:10.1016/j.foodchem.2014.08.092

21. Choi DH, Lee SK, Oh YK, et al. A dual gold nanoparticle conjugate-based lateral flow assay (LFA) method for the analysis of troponin I. *Biosens Bioelectron*. 2010;25(8):1999–2002. doi:10.1016/j.bios.2010.01.019
22. Guo JC, Chen SQ, Guo JH, Ma X. Nanomaterial labels in lateral flow immunoassays for point-of-care-testing. *J Mater Sci Technol*. 2021;60:90–104. doi:10.1016/j.jmst.2020.06.003
23. Perfezou M, Turner A, Merkoci A. Cancer detection using nanoparticle-based sensors. *Chem Soc Rev*. 2012;41(7):2606–2622. doi:10.1039/c1cs15134g
24. Wu L, Qu XG. Cancer biomarker detection: recent achievements and challenges. *Chem Soc Rev*. 2015;44(10):2963–2997. doi:10.1039/c4cs00370e
25. Vidotti M, Carvalhal RF, Mendes RK, Ferreira DCM, Kubota LT. Biosensors based on gold nanostructures. *J Braz Chem Soc*. 2011;22(1):3–20. doi:10.1590/S0103-50532011000100002
26. Li Y, Zhou Y, Chen X, Huang X, Xiong Y. Comparison of three sample addition methods in competitive and sandwich colloidal gold immunochromatographic assay. *Anal Chim Acta*. 2020;1094:90–98. doi:10.1016/j.aca.2019.09.079
27. Parveen R, Ullah S, Sgarbi R, Tremiliosi-Filho G. One-pot ligand-free synthesis of gold nanoparticles: the role of glycerol as reducing-cum-stabilizing agent. *Colloids Surf A*. 2019;565:162–171. doi:10.1016/j.colsurfa.2019.01.005
28. Amstad E, Textor M, Reimhult E. Stabilization and functionalization of iron oxide nanoparticles for biomedical applications. *Nanoscale*. 2011;3(7):2819–2843. doi:10.1039/c1nr10173k
29. Wang YT, Lu XM, Zhu F, Zhao M. The preparation of gold nanoparticles and evaluation of their immunological function effects on rats. *Biomed Mater Eng*. 2014;24(1):885–892. doi:10.3233/bme-130882
30. Rodriguez-Montelongo SA, Gonzalez-Hernandez J, Macias AH, et al. Synthesis, characterization, and toxicity of hollow gold nanoshells. *J Nanopart Res*. 2018;20(11):311. doi:10.1007/s11051-018-4420-2
31. Schwartzberg AM, Olson TY, Talley CE, Zhang JZ. Synthesis, characterization, and tunable optical properties of hollow gold nanospheres. *J Phys Chem B*. 2006;110(40):19935–19944. doi:10.1021/jp062136a
32. Glavee GN, Klabunde KJ, Sorensen CM, Hadjipanayis GC. Borohydride reduction of cobalt ions in water. Chemistry leading to nanoscale metal, boride, or borate particles. *Langmuir*. 1993;9(1):162–169. doi:10.1021/la00025a034
33. Huang ZB, Xu Y, Li LS, Li YP, Zhang H, He QH. Development of an immunochromatographic strip test for the rapid simultaneous detection of deoxynivalenol and zearalenone in wheat and maize. *Food Control*. 2012;28(1):7–12. doi:10.1016/j.foodcont.2012.04.035
34. Xu Y, Huang ZB, He QH, Deng SZ, Li LS, Li YP. Development of an immunochromatographic strip test for the rapid detection of deoxynivalenol in wheat and maize. *Food Chem*. 2010;119(2):834–839. doi:10.1016/j.foodchem.2009.08.049
35. Long JW GL. Limit of detection A closer look at the IUPAC definition. *Anal Chem*. 1983;55: doi:10.1021/ac00258a001
36. Altman DG, Bland JM. Measurement in medicine: the analysis of method comparison studies. *Statistician*. 1983;32(3): 1
37. Bland JM, Altman DG. Statistical methods for assessing agreement between two methods of clinical measurement. *Int J Nurs Stud*. 2010;47(8):931–936. doi:10.1016/j.ijnurstu.2009.10.001
38. Thobhani S, Attree S, Boyd R, et al. Bioconjugation and characterisation of gold colloid-labelled proteins. *J Immunol Methods*. 2010;356(1–2):60–69. doi:10.1016/j.jim.2010.02.007
39. Safenkova IV, Zherdev AV, Dzantiev BB. Factors influencing the detection limit of the lateral-flow sandwich immunoassay: a case study with potato virus X. *Anal Bioanal Chem*. 2012;403(6):1595–1605. doi:10.1007/s00216-012-5985-8
40. Cruje C, Chithrani BD. Integration of peptides for enhanced uptake of PEGylayed gold nanoparticles. *J Nanosci Nanotechnol*. 2015;15(3):2125–2131. doi:10.1166/jnn.2015.10321
41. Xu W, Chen X, Huang X, et al. Ru(phen)3(2+) doped silica nanoparticle based immunochromatographic strip for rapid quantitative detection of beta-agonist residues in swine urine. *Talanta*. 2013;114:160–166. doi:10.1016/j.talanta.2013.04.013
42. Dhingra R, Gona P, Nam BH, et al. C-reactive protein, inflammatory conditions, and cardiovascular disease risk. *Am J Med*. 2007;120(12):1054–1062. doi:10.1016/j.amjmed.2007.08.037